



Type of the Paper (Article, or Communication)

Photonic band gaps and resonance modes in 2D twisted moiré photonic crystal

Khadijah Alnasser¹, Steve Kamau,¹ Noah Hurley,¹ Jingbiao Cui,¹ and Yuankun Lin^{1,2,*}

- ¹Department of Physics, Univ. of North Texas, Denton, TX 76203, USA; KhadijahAlnasser@my.unt.edu (K.A.); SteveKamau@my.unt.edu (S.K.); noahhurley@my.unt.edu (N.H.); Iingbiao.Cui@unt.edu (J.C.)
- ² Department of Electrical Engineering, Univ. of North Texas, Denton, TX 76203, USA.
- * Correspondence: yuankun.lin@unt.edu; Tel.: +1-940-565-4548

Abstract: The study on twisted bilayer 2D materials has revealed many interesting physics. The twisted moiré photonic crystal is an optical analog of twisted bilayer 2D materials. The optical properties in twisted photonic crystals have not been fully understood yet. In this paper, we generate 2D twisted moiré photonic crystals without physical rotation, and simulate their photonic band gaps in photonic crystals formed at different twisted angles, different gradient levels and different dielectric filling factors. At certain gradient levels, interface modes appear within the photonic band gap. The simulation reveals "tic tac toe" like and "traffic circle" like modes, and ring resonance mode. These interesting discoveries in 2D twisted moiré photonic crystal can lead toward its application in integrated photonics.

Keywords: Moiré photonic crystal; twisted photonic crystal; photonic band gap; graded photonic super-crystal; interface mode

1. Introduction

Reducing the dimensionality of a material system leads very often to exceptional electronic, optical, and magnetic properties because of enhanced quantum effects in reduced phase space [1]. Recently, atomically thin two-dimensional (2D) materials can be stacked layer-by-layer to create synthetic materials with entirely new properties [2]. Intensive researches have been focused on moiré materials where 2D layered materials are superposed against each other with a relative twist angle [3-18]. The formed moiré pattern at different twist angles has resulted in topological edge state, formation of moiré excitons, interlayer magnetism and fine control of the electron band structure [3-18]. Especially, the recent discovery of superconductivity in magic-angle twisted bilayer graphene [4] has triggered another wave of researches in moiré 2D materials [5-18].

Twisted moiré photonic crystal is an optical analog of twisted 2D materials while photonic crystal is a periodic dielectric structure with a modulation of the refractive index close to operation wavelength of light [19-21]. The twisted bilayer photonic crystal is consisted of two layers of identical photonic crystal stacked into moiré patterns [19, 22-24] that have also revealed magic-angle photonic flat bands with a non-Anderson-type localization [23]. Several research groups have generated twisted photonic crystals in photore-fractive crystals with a shallow refractive index modulation and have observed the localization and delocalization of light waves [25-31]. The moiré photonic crystals have also been fabricated by holographic fabrication through laser interference of two sets of laser beams arranged in two-cone geometry with different cone angles [31-38]. Due to the gradient pattern and super-cell in the photonic crystal, it has also been named as graded photonic super-crystal [37-39] or graded photonic super-quasi-crystal [35]. In contrast to twisted bilayer 2D materials and twisted bilayer photonic crystal, two mutually twisted

Photonics 2021, 8, x. https://doi.org/10.3390/xxxxx

optical lattices generated by laser interference will interfere further and form single layer twisted photonic crystal if we consider 2D case [36].

In this paper, we show the relationship between moiré pattern and twisted holographic pattern. Due to three-dimensional (3D) feature in the formed holographic pattern, there are different modulation levels at different z-locations thus different gradient in x-y plane. We simulate photonic band structure and resonance modes for 2D twisted photonic crystal formed at different z-locations. There are interface modes within the photonic band gap at certain z-locations. Interestingly, crossing waveguide along the interface, ring resonator and their combination appears at different frequencies in the simulation of electric-field intensity for resonance modes in the 2D twisted moiré photonic crystal.

2. Design principle from a moiré pattern with a physical rotation to a twisted holographic photonic crystal without physical rotations

The design principle of twisted photonic crystals comes from the analysis of reciprocal spatial and frequency (spectral) domains of the moiré pattern and the application of such an analysis to the real and reciprocal k-space in optical lattice.

Figure 1(a) shows the superposition of 2D square dot patterns in spatial domain, as an example, with a twist angle of α . The square dot pattern edged by a yellow square in Fig. 1(a) has two fundamental frequency vectors f_1 and f_2 in spectral domain in the Fourier transform. These two frequency vectors are perpendicular and have the same magnitude as shown in Fig. 1(b). The spectra of Fourier transform have ..., -3f₁, -2f₁, -f₁, 0, f₁, 2f₁, 3f₁,... and -3f₂, -2f₂, -f₂, 0, f₂, 2f₂, 3f₂, ..., etc. [40]. Only frequency vectors of -f₁, f₁ and -f₂, f₂ are drawn in purple arrows in Fig. 1(b). For the square dot pattern edged by a blue square, only frequency vectors of -f₃, f₃ and -f₄, f₄ are drawn in blue arrows in Fig. 1(b). f₃, and f₄ vectors are perpendicular and have the same magnitude. Frequencies of f₁-f₃ and f₂-f₄ in Fig. 1(b) are within the visible circle [40]. The spectra with frequencies of f₁-f₃ and f₂-f₄ represent the visible periodic component in spatial domain in Fig. 1(a). The index for a moiré pattern is defined by, for example, f₁-f₃=(1f₁+0f₂-f₃+0f₄) => (1,0,-1,0) [40]. Thus Fig. 1(a) shows a moiré pattern with an index of (1,0,-1,0) and (0,1,0,-1) in the superposition of two square dot patterns with a twist angle of α . The moiré frequency (f₁-f₃) can be calculated by Eq. (1)

$$f_1 - f_3 = 2f_1 \sin \frac{\alpha}{2}$$
 (1)

Similar analysis is applied to the holographic pattern below. When eight beams (eight 532 nm green spots in Fig. 1(c)) are overlapped through 4f imaging system [34], these four inner beams together with four outer beams have holographic interference with an intensity I(r) calculated by Eq. (2):

$$I(r) = \langle \sum_{i=1}^{8} E_i^2(r,t) \rangle + \sum_{i < j}^{8} E_i E_j e_i \cdot e_j \cos \left[\left(k_j - k_i \right) \cdot r + \left(\delta_j - \delta_i \right) \right]. \tag{2}$$

where e is the electric field polarization, E is the electric field, k is the wave vector, and δ is the initial phase. The orientation of the optical lattice in real space is determined by the vector difference of (k_1-k_k) in reciprocal space. (k_1,k_2,k_3,k_4) in Fig. 1(c) are the k-vector components in x-y plane for outer beams and have the same magnitude while (k_5,k_6,k_7,k_8) are the k-vector components in x-y plane for inner beams and have also the same magnitude. From Fig. 1(c), we can see that the k-vector difference (k_1-k_6) is twisted by a rotation angle α from (k_3-k_6) . There is a same twist angle between (k_2-k_7) and (k_4-k_7) , between (k_3-k_8) and (k_1-k_8) , and between (k_4-k_5) and (k_2-k_5) . By analyzing the cross-section in x-y plane of formed 3D holographic pattern, square optical lattice in real space due to reciprocal k-vectors of (k_1-k_6) , (k_2-k_7) , (k_3-k_8) , and (k_4-k_5) is twisted by a rotation angle α from those by (k_3-k_6) , (k_4-k_7) , (k_1-k_8) and (k_2-k_5) . The twist angle α is determined by the ratio of k-vector component in x-y plane of the inner beam over the outer beam in Eq. (3):

$$\alpha = 2 \tan^{-1} \left(\frac{k_6}{k_1} \right) \quad (3)$$

Fig. 1(d) shows a simulated twisted 2D holographic photonic crystal in x-y plane. Super-cell appears in the figure as indicated by red solid square. The size (s) of super-cell is approximately determined by Eq. (4):

$$s = \frac{2\pi}{k_5 \cos 45 - k_6 \cos 135} = \frac{2\pi}{2k_6 \cos 45} \tag{4}$$

and lattice period a is approximately calculated by Eq. (5):

$$a = \frac{2\pi}{k_1 \cos 45 - k_2 \cos 135} = \frac{2\pi}{2k_1 \cos 45}$$
 (5)

So the size of super-cell is related to lattice period a and twist angle α by Eq. (6):

$$s = \frac{k_1}{k_6} a = \frac{a}{\tan(\frac{\alpha}{2})}$$
 (6)

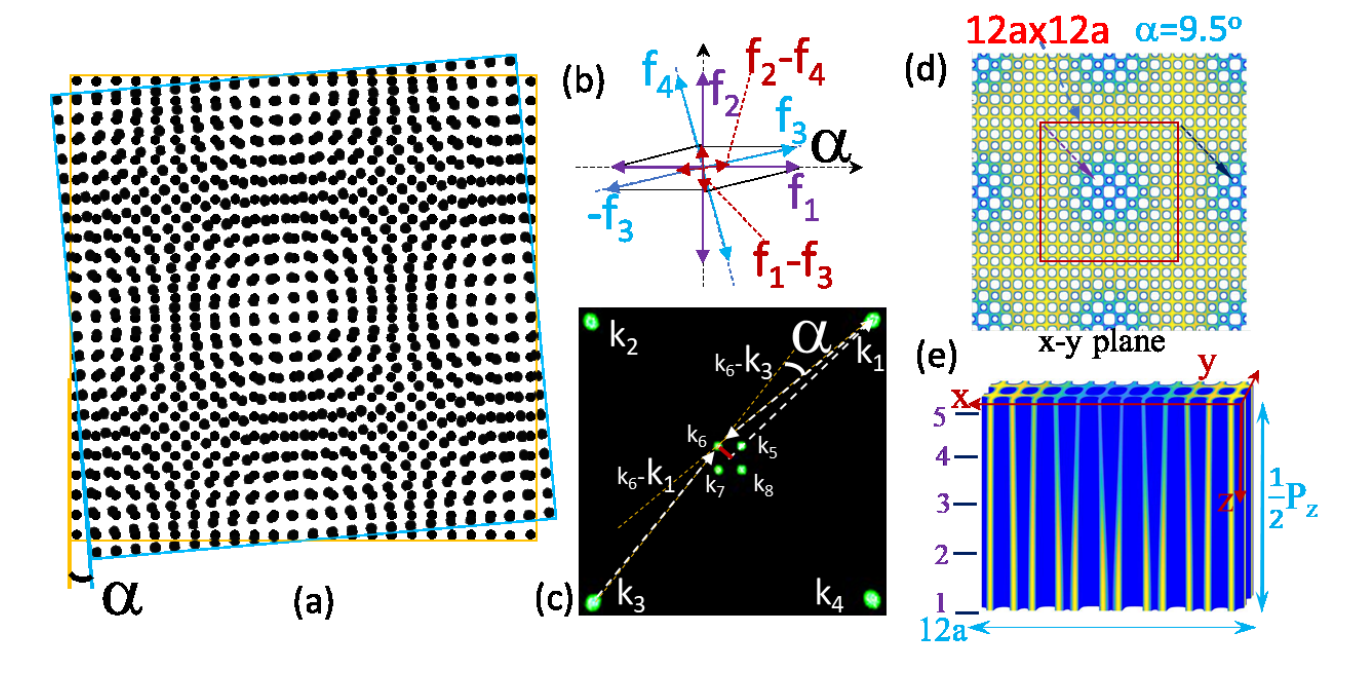


Fig. 1. (a) A ((1,0,-1,0), (0,1,0,-1)) moiré in the superposition of two square dot patterns with a twist angle of α, (b) and its first-order spectra; (c) Components of k-wavevectors in x-y plane for 8 interfering beams before their overlapping; (d) Inverted 2D moiré interfere pattern with a twist angle of 9.5 degrees and super-cell size of 12a×12a; (e) Inverted 3D interfere pattern. The label of 1, 2, 3, 4 and 5 indicate the z-locations from the bottom.

The period in z-direction (P_z) of the 3D holographic pattern is determined by the z-components of inner and outer beams, $k_{i,z}$ and $k_{o,z}$, respectively, in Eq. (7):

$$P_z = \frac{2\pi}{k_{l,z} - k_{0,z}} \tag{7}$$

Fig. 1(d) shows simulated 2D moiré photonic crystal in x-y plane with a twist angle of 9.5 degrees and super-cell size of 12a×12a as indicated by the solid red square. The central area of the red square in Fig. 1(d) is a bright region and others are dark regions. Fig. 1(e) shows 3D interference pattern with a dimension of 12a×2a×0.5Pz. These two figures are inverted structures from the interference assuming a positive photoresistor is used. Fig. 1(d) is a cross section at z=0.17Pz from the bottom of Fig. 1(e).

Thus, by arranging the two sets of interfering beams in two-cone geometry and controlling the cone angle, we are able to relate the moiré pattern to the twist photonic crystal.

Those graded photonic super-crystals [31,33,34,37] generated by two-cone arrangement of laser beam are actually 2D twisted photonic crystals.

3. Simulation methods

We simulate photonic band gap and resonance modes for 2D twist moiré photonic crystal obtained at different z-locations of 1, 2, 3, 4 and 5 in Fig. 1(e) and also at different iso-intensity surface by setting-up the intensity threshold. In the simulation, the interference intensity function, I(r), in Eq. (2) at certain z-location, is replaced by a binary Si/air structures by comparing I(r) with a threshold intensity Ith. A step function is used: $\epsilon(r) = 1$ (for air) when I> Ith, and $\epsilon(r) = 12$ (for Si) when I<Ith. Photonic band structures in 2D twisted moiré photonic crystal with air holes in Si were computed using the MIT Photonic Bands (MPB) software package, a fully-vectorial eigenmode solver for Maxwell's equations [41], via Simpetus Electromagnetic Simulation Platform from Amazon Web Services. The spatial distribution of dielectric constants was output from MPB and is shown in top row in Fig. 2 at different z-locations of 0.11, 0.23, 0.34 and 0.45Pz in location 2, 3, 4 and 5 in Fig. 1(e), respectively. We also simulate cavity quality factors and electric field (E-field) intensity distributions for resonance modes in twisted photonic crystal with a thickness of 2a using the harmonic inversion function included in the MIT MEEP software [42,43] via Amazon Web Services.

3. Results

3.1. Photonic band structures in twisted photonic crystals with different z-locations, twist angle and threshold intensity in the step function

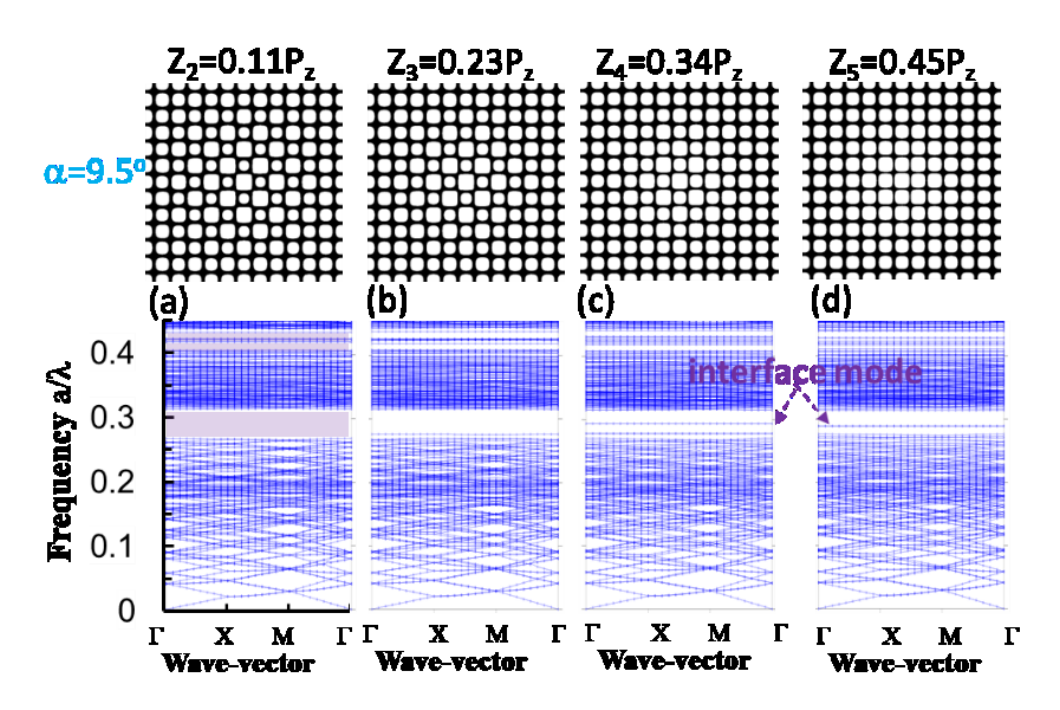


Figure 2. (Top row) Iso-intensity slices produced from the eight-beam interference with a twist angle of 9.5 degrees and used as an unit super-cell to calculate the respective photonic band structures for TE modes in (a,b,c,d) (bottom row) at z-locations of 0.11, 0.23, 0.34 and 0.45Pz, respectively.

We have simulated photonic band structures in moiré photonic crystals with a twist angle of 9.5 degree obtained at various z-locations. Figs. 2 (a,b,c,d) show the results for TE modes in the twisted moiré photonic crystals at z=0.11, 0.23, 0.34 and 0.45 P_z , respectively. The smaller the z-location in Fig. 2, the higher the gradient level is. The shadowed areas in Fig. 2(a) indicate the photonic crystal gaps. Fig. 2(a) shows three photonic band gaps

around frequency a/λ of 0.26-0.31, 0.4-0.42, and 0.43-0.44. With increasing z-location, the size of all three band gaps decrease and frequency ranges of photonic band gaps are almost same. However, interface modes (or called waveguide mode for wave propagation) appear within the lowest photonic band gap in Figs. 2(c,d). The photonic band gap around 0.4-0.41 disappears at z-location=0.45Pz in Fig. 2(d).

Fig. 3 shows the photonic band structure for TE modes in moiré photonic crystals with twist angles of 6.4, 9.5 and 18.9 degrees at z-location around 0.4Pz. In Fig. 3(a) and 3(b), the photonic band gap appears at almost same frequency range and almost same gap size. Interface modes appear in both Fig. 3(a) and 3(b). In the unit super-cell of 12a×12a in Fig. 3(b), half of lattices are inside the yellow circle (bright region). Both dark and bright regions have contribution to the formation of photonic band gap and interface mode. An increase of the unit super-cell to 18a×18a in Fig. 3(a) only increases the dark region outside the yellow circle. However, almost all regions are considered as bright region in the unit super-cell of 6a×6a in Fig. 3(c). The photonic band gap increases and interface mode is not flat and close to the band-edge above the shadowed area in Fig. 3(c). Other optical property, such as extraction efficiency of organic light emitting diode patterned in moiré photonic crystal, reaches high performance in moiré photonic crystal with unit super-cell sizes between 9a×9a and 14a×14a [44]. It is not necessary to have a twisted photonic crystal with a very large unit super-cell in order to gain different properties from traditional photonic crystal. Below we focus our research on the moiré photonic crystal with a twist angle of 9.5 degree (super-cell of 12a×12a).

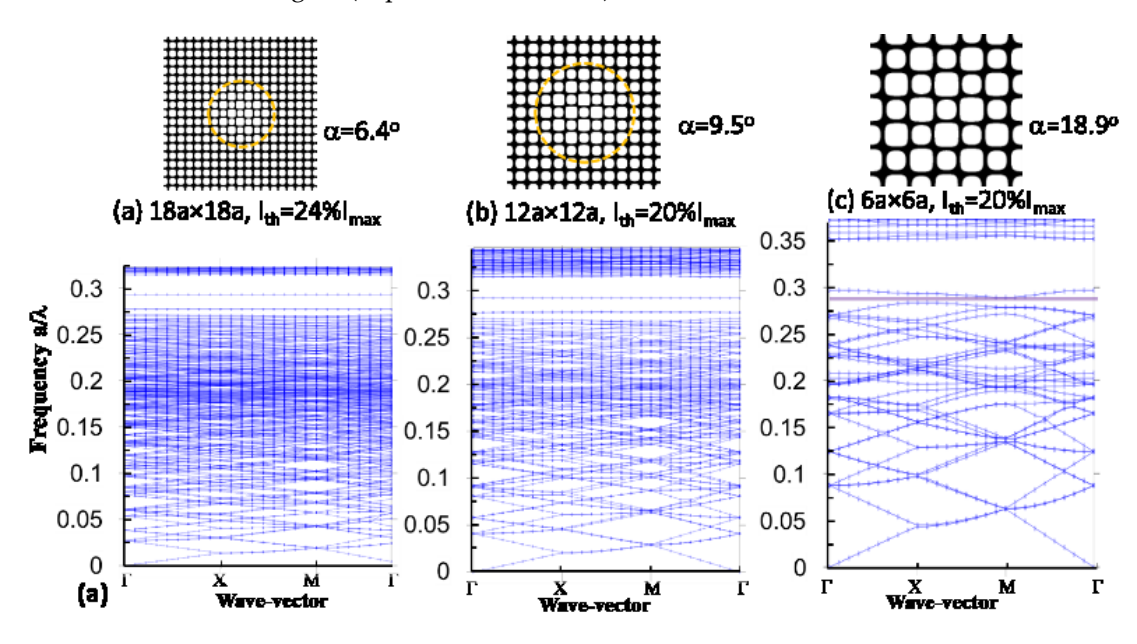


Figure 3. (Top row) Iso-intensity slices produced from the eight-beam interference at certain threshold intensity with twist angles of 6.4 (a), 9.5 (b) and 18.9 degrees (c) and used as a unit super-cell to calculate the respective photonic band structures for TE modes (bottom row) at z-locations around 0.4Pz.

We have simulated photonic band structures for moiré photonic crystals with a twist angle of 9.5 degree, obtained by setting threshold I_{th} in the range of $16\%I_{max}$ and $26\%I_{max}$ in the step function and at z-locations of 0.11, 0.23, 0.34 and 0.45Pz. Representative results for twisted photonic crystals with z=0.11Pz, $I_{th}=16\%I_{max}$ and $24\%I_{max}$ are shown in Fig. 4(a) and 4(b), and with z=0.34Pz, $I_{th}=18\%I_{max}$ and $24\%I_{max}$ in Fig. 4(c) and 4(d), respectively. With increasing threshold intensity, both filling fraction of dielectric materials and effective refractive index of the twisted photonic crystal will increase. The central wavelength for the Bragg diffraction from the twisted photonic crystal will also increases. Thus the central frequency of the photonic band gap decreases as shown in Fig. 4. The band gap width also decreases with increasing threshold intensity. By varying I_{th} , the bottom photonic band

Wave-vector

gap does not have an interface mode for twisted photonic crystals obtained at z=0.11 and $0.23P_z$ and there is always an interface mode in the bottom band gap for those obtained at z=0.34 and $0.45P_z$. However, the band gap splits and interface modes appear in upper band gap with increasing I_{th} for all z locations.

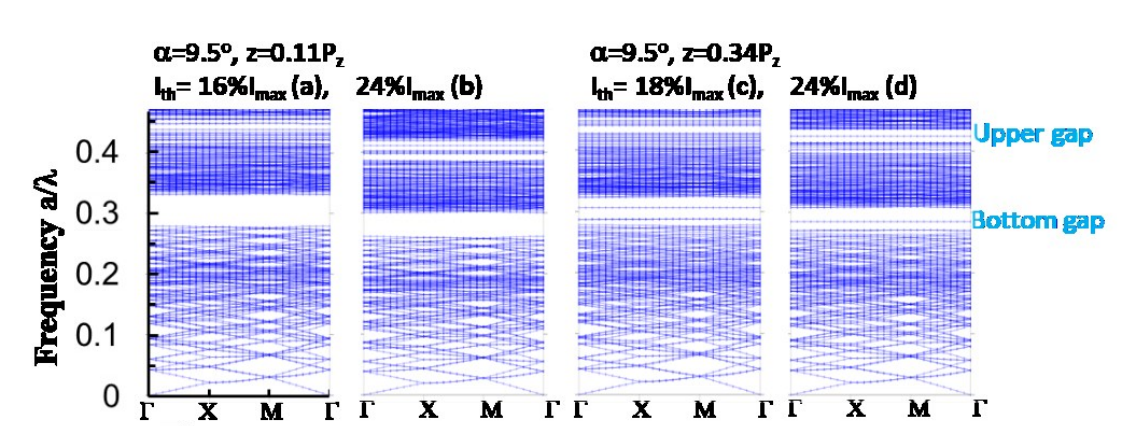


Figure 4. Photonic band structures for TE modes in moiré photonic crystal with a twist angle of 9.5 degree at a z-location of 0.11Pz and with a threshold intensity of 16%I_{max} (a) and 24%I_{max} (b), and at a z-location of 0.34Pz and with a threshold intensity of 18%I_{max} (c) and 24%I_{max} (d).

3.2. Resonance modes in twisted photonic crystals at different z-locations

We simulate quality-factors (Q-factors) and electric-field intensity distribution for resonance modes in two moiré photonic crystals where one has no interface mode and the other has an interface mode in the bottom band gap. Fig. 5(a-f) shows electric-field intensity for resonance and interface modes at frequency a/λ of 0.285, 0.30, 0.39, 0.40, 0.414 and 0.42 with a Q-factor of 45888, 2691, 1226, 6817, 2150 and 1683, respectively, for moiré photonic crystal with a twist angle of 9.5 degree at z=0.11Pz. Due to the dislocation in the bottom band gap [38] between the bright and dark regions in the moiré photonic crystal, some resonance modes appear in the bright region with a high Q-factor as shown in Fig. 5(a). The resonance or waveguide modes in Fig. 5(c-f) are related to the interface modes in the upper band gap. They have a square symmetry with oscillations in x and y directions in Fig. 5(c), in diagonal direction in 5(f) and in both x (or y) and diagonal directions in 5(d-e). Fig. 5(g) shows Q-factors for resonance and interface modes at certain frequency locations. The purple square and red circles in the figure indicate these modes near the band gap edges or within the interface state.

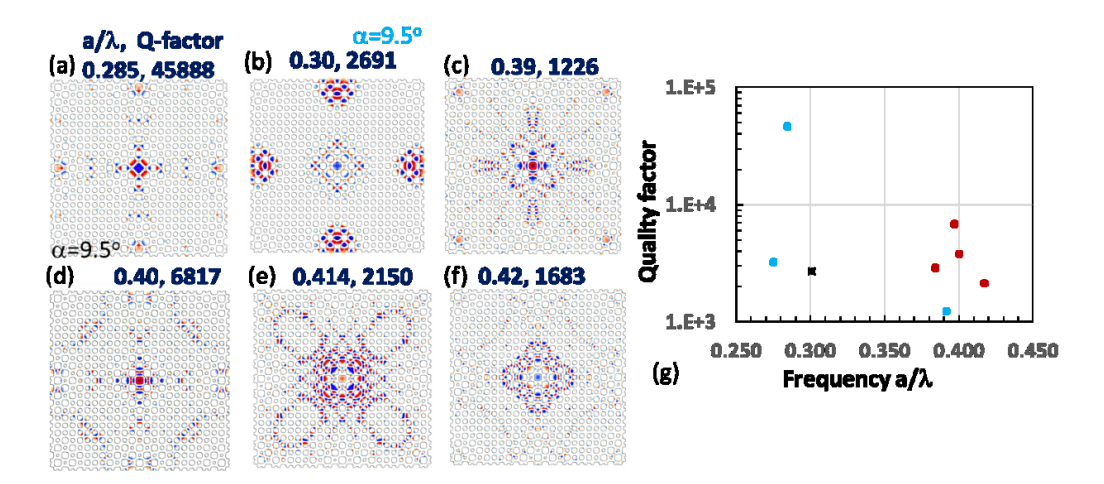


Figure 5. Simulated electric field intensity for resonance modes in the moiré photonic crystal with a twist angle of 9.5° obtained at $z=0.11P_z$ and $I_{th}=24\%I_{max}$. Frequency a/λ and Q-factor are labelled in each figure (a-f). (g) Calculated Q-factors at certain frequencies for resonance modes in the moiré photonic crystal with a twist angle of 9.5 degrees.

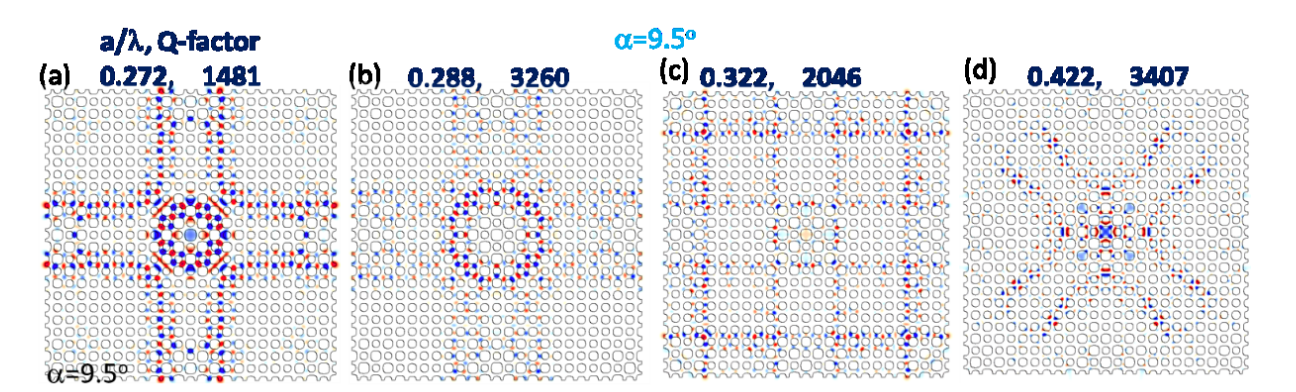


Figure 6. (a-d) Simulated electric field intensity for resonance modes in the moiré photonic crystal with a twist angle of 9.5° obtained at z=0.34Pz and I_{th}=26%I_{max}. Frequency a/λ and Q-factor are labelled in each figure.

Fig. 6 shows electric-field intensity distribution for interface (or waveguide) modes at frequency a/λ of 0.272, 0.288, 0.322, and 0.422 with a Q-factor of 1481, 3260, 2046 and 3407, respectively, for moiré photonic crystal with a twist angle of 9.5 degree at z=0.34Pz. Due to the small gradient in the moiré pattern at z=0.34Pz and interface modes within both bottom and upper band gaps, wave propagation into the moiré photonic crystal is expected. High symmetry "traffic circle" like waveguide and ring resonator are observed in Fig. 6(a) at a frequency a/λ of 0.272, close to the frequency for the interface mode within the bottom band gap. Fig. 6(b) shows a ring resonator around the edge of the bright region in the moiré photonic crystal at a frequency a/λ of 0.288. Square symmetry "tic tac toe" like wave propagation is shown in Fig. 6(c) at a frequency a/λ of 0.322, near the gap edge of bottom band gap. The "x" shape resonance mode in Fig. 6(d) corresponds to the interface mode within the upper band gap.

4. Discussion

Usually point or line defects are designed for the engineering of resonance cavity or waveguide in the traditional photonic crystal. In the moiré photonic crystal with a twist angle of 9.5 degree in Fig. 6, there is an interface for light to propagate without specifically designed defects in the twisted photonic crystal. Topological properties in moiré photonic crystals need to be further studied for a potential application of topological waveguide [45,46].

The pattern inside the red square in Fig. 1(d) with a size of 12a×12a has been input as a unit super-cell for the simulation of photonic band gap. The size of air motif increases along the purple dashed arrow in diagonal direction in the figure. However, the size of air motif decreases along the blue dashed arrow on the right side of the square in Fig. 1(d). In order to have more accurate photonic band structure in the moiré photonic crystal, a unit super-cell of 24a×24a can be used for the simulation. However, higher performance computation than the current one is needed. Even for the current simulation with a unit super-cell of 12a×12a, the resolution of 18 is not high enough.

The simulation of electric-field intensity and Q-factors has been performed in a pattern with a size of 24a×24a for the twisted photonic crystal with a unit super-cell size of 12a×12a in Fig. 5 and Fig. 6. These results have included the effect of size changes in air motif in Fig. 1(d).

We have not understood yet why we are not able to obtain photonic band gaps for TM modes by varying the threshold intensity thus the filling fraction of dielectric materials. With increasing unit super-cell size, the number of modes increases per a frequency

range in the photonic band structure. With the same unit super-cell size, the number of modes per a frequency range is same in twisted photonic crystals obtained by different z-locations in Fig. 2. The central wavelength of the photonic band gap is scalable with the lattice constant of the twisted photonic crystal. A change of refractive index in dielectric materials in twisted photonic crystal will not only shift the central frequency of band gap but also change the band gap size. For the simulation of photonic band gap of twisted photonic crystals in dielectric materials with varying refractive index at different wavelength, a MEEP program should be used [38,47]. However, the MEEP program is not good at simulating the photonic band structure at low frequencies.

5. Conclusions 271

We have revealed the relationship between moiré patterns and twisted photonic crystals through analysis of moiré patterns in reciprocal spatial and spectral domains and holographic pattern in reciprocal spatial and wavevector spaces. The twist angle of moiré photonic crystal has been calculated from the wavevector of interfering beams arranged in dual-cone geometry. We have simulated photonic band gap, electric field intensity distribution for resonance modes and their Q-factors in twisted photonic crystal at different twist angle, different z-locations (different gradient) and different iso-intensity levels. At certain gradient in moiré twisted photonic crystals, we have observed interface modes within the photonic band gap and various wave-propagation and resonances including ring-resonators and "traffic circle" like pattern. Further study can lead toward the application of twisted photonic crystals in integrated photonics.

Author Contributions: Conceptualization, Y.L. and J.C.; methodology, Y.L., K.A., S.K. and N.H; software, K.A., and S.K.; formal analysis, Y.L. and K.A.; writing—original draft preparation, K.A. and Y.L.; writing—review and editing, N.H.; funding acquisition, J.C. and Y.L. All authors have read and agreed to the published version of the manuscript.

Funding: This research was funded by the U.S. National Science Foundation, grant number 2128367.

Conflicts of Interest: The authors declare no conflict of interest. The funders had no role in the design of the study; in the collection, analyses, or interpretation of data; in the writing of the manuscript, or in the decision to publish the results.

Data Availability Statement: Data will be available upon request.

References

- 1. Geim, A. K.; Novoselov, K. S. The Rise of Graphene. Nat. Mater. 2007, 6 (3), 183–191.
- 2. Woods, C. R.; Britnell, L.; Eckmann, A.; Ma, R. S.; Lu, J. C.; Guo, H. M.; Lin, X.; Yu, G. L.; Cao, Y.; Gorbachev, R. V. Commensurate–Incommensurate Transition in Graphene on Hexagonal Boron Nitride. Nat. Phys. 2014, 10 (6), 451–456.
- 3. Carr, S.; Massatt, D.; Fang, S.; Cazeaux, P.; Luskin, M.; Kaxiras, E. Twistronics: Manipulating the Electronic Properties of Two-Dimensional Layered Structures through Their Twist Angle. Phys. Rev. B 2017, 95 (7), 075420.
- 4. Cao, Y.; Fatemi, V.; Fang, S.; Watanabe, K.; Taniguchi, T.; Kaxiras, E.; Jarillo-Herrero, P. Unconventional Superconductivity in Magic-Angle Graphene Superlattices. Nature 2018, 556 (7699), 43–50.
- 5. Burg, G. W.; Zhu, J.; Taniguchi, T.; Watanabe, K.; MacDonald, A. H.; Tutuc, E. Correlated Insulating States in Twisted Double Bilayer Graphene. Phys. Rev. Lett. 2019, 123 (19), 197702.
- 6. Yankowitz, M.; Chen, S.; Polshyn, H.; Zhang, Y.; Watanabe, K.; Taniguchi, T.; Graf, D.; Young, A. F.; Dean, C. R. Tuning Superconductivity in Twisted Bilayer Graphene. Science 2019, 363 (6431), 1059–1064.
- 7. Arora, H. S.; Polski, R.; Zhang, Y.; Thomson, A.; Choi, Y.; Kim, H.; Lin, Z.; Wilson, I. Z.; Xu, X.; Chu, J.-H.; Watanabe, K.; Taniguchi, T.; Alicea, J.; Nadj-Perge, S. Superconductivity in Metallic TWISTED Bilayer GRAPHENE Stabilized by WSe2. Nature 2020, 583, 379–384.
- 8. Balents, L.; Dean, C. R.; Efetov, D. K.; Young, A. F. Superconductivity and Strong Correlations in Moiré Flat Bands. Nat. Phys. 2020, 16 (7), 725–733.
- 9. Gonzalez, J.; Stauber, T. Kohn-Luttinger Superconductivity in Twisted Bilayer Graphene. Phys. Rev. Lett. 2019, 122 (2), 026801.
- Bai, Y.; Zhou, L.; Wang, J.; Wu, W.; McGilly, L. J.; Halbertal, D.; Lo, C. F. B.; Liu, F.; Ardelean, J.; Rivera, P., et al. Excitons in strain-induced one-dimensional moir e potentials at transition metal dichalcogenide heterojunctions. Nat. Mater. 2020, 19, 1068– 1073.

2- 263 e 264 c 265 p 266

- 11. Chen, S.; He, M.; Zhang, Y.-H.; Hsieh, V.; Fei, Z.; Watanabe, K.; Taniguchi, T.; Cobden, D. H.; Xu, X.; Dean, C. R. Electrically Tunable Correlated and Topological States in Twisted Monolayer–Bilayer Graphene. Nat. Phys. 2021, 17 (3), 374–380.
- 12. Hu, G.; Ou, Q.; Si, G.; Wu, Y.; Wu, J.; Dai, Z.; Krasnok, A.; Mazor, Y.; Zhang, Q.; Bao, Q. Topological Polaritons and Photonic Magic Angles in Twisted α-MoO 3 Bilayers. Nature 2020, 582 (7811), 209–213.
- 13. Carr, S.; Fang, S.; Kaxiras, E. Electronic-Structure Methods for Twisted Moiré Layers. Nat. Rev. Mater. 2020, 5 (10), 748–763.
- 14. Zhang, Z.; Wang, Y.; Watanabe, K.; Taniguchi, T.; Ueno, K.; Tutuc, E.; LeRoy, B. J. Flat Bands in Twisted Bilayer Transition Metal Dichalcogenides. Nat. Phys. 2020, 16 (11), 1093–1096.
- 15. Hu, G.; Krasnok, A.; Mazor, Y.; Qiu, C.-W.; Alù, A. Moiré Hyperbolic Metasurfaces. Nano Lett. 2020, 20 (5), 3217–3224.
- 16. He, M.; Li, Y.; Cai, J.; Liu, Y.; Watanabe, K.; Taniguchi, T.; Xu, X.; Yankowitz, M. Symmetry Breaking in Twisted Double Bilayer Graphene. Nat. Phys. 2021, 17 (1), 26–30.
- 17. Xu, S.; Al Ezzi, M. M.; Balakrishnan, N.; Garcia-Ruiz, A.; Tsim, B.; Mullan, C.; Bar- rier, J.; Xin, N.; Piot, B. A.; Taniguchi, T.; Katayama, K.; Carvalho, A.; Mishchenko, A.; Geim, A.; Fal'ko, V.; Adam, S.; Neto, A. H. C.; Novoselov, K. & Shi, Y. Tunable van Hove singularities and correlated states in twisted monolayer–bilayer graphene. Nat. Phys. 2021, 17, 619–626.
- 18. Slizovskiy, S.; Garcia-Ruiz, A.; Berdyugin, A.; Xin, N.; Taniguchi, T.; Watanabe, K.; Geim, A.; Drummond, N.; Fal'ko, V. Out-of-Plane Dielectric Susceptibility of Graphene in Twistronic and Bernal Bilayers. Nano Lett. 2021, 21, 6678–6683.
- 19. Lou, B.; Zhao, N.; Minkov, M.; Guo, C.; Orenstein, M.; Fan, S. Theory for Twisted Bilayer Photonic Crystal Slabs. Phys. Rev. Lett. 2021, 126 (13), 136101.
- 20. Sunku, S. S.; Ni, G.; Jiang, B.-Y.; Yoo, H.; Sternbach, A.; McLeod, A. S.; Stauber, T.; Xiong, L.; Taniguchi, T.; Watanabe, K. Photonic Crystals for Nano-Light in Moiré Graphene Superlattices. Science 2018, 362 (6419), 1153–1156.
- 21. Hu, G.; Ou, Q.; Si, G.; Wu, Y.; Wu, J.; Dai, Z.; Krasnok, A.; Mazor, Y.; Zhang, Q.; Bao, Q. Topological Polaritons and Photonic Magic Angles in Twisted *α*-MoO 3 Bilayers. Nature 2020, 582 (7811), 209–213.
- Wu, Z.; Zheng, Y. Moiré Chiral Metamaterials. Adv. Opt. Mater. 2017, 5 (16), 1700034.
- 23. Dong, K.; Zhang, T.; Li, J.; Wang, Q.; Yang, F.; Rho, Y.; Wang, D.; Grigoropoulos, C. P.; Wu, J.; Yao, J. Flat Bands in Magic-Angle Bilayer Photonic Crystals at Small Twists. Phys. Rev. Lett. 2021, 126 (22), 223601.
- 24. Hu, G.; Zheng, C.; Ni, J.; Qiu, C.-W.; Alù, A. Enhanced Light-Matter Interactions at Photonic Magic-Angle Topological Transitions. Appl. Phys. Lett. 2021, 118 (21), 211101.
- 25. Huang, C.; Ye, F.; Chen, X.; Kartashov, Y. V.; Konotop, V. V.; Torner, L. Localization-Delocalization Wavepacket Transition in Pythagorean Aperiodic Potentials. Sci. Rep. 2016, 6 (1), 1–8.
- 26. Wang, P.; Zheng, Y.; Chen, X.; Huang, C.; Kartashov, Y. V.; Torner, L.; Konotop, V. V.; Ye, F. Localization and Delocalization of Light in Photonic Moiré Lattices. Nature 2020, 577 (7788), 42–46.
- 27. Fu, Q.; Wang, P.; Huang, C.; Kartashov, Y. V.; Torner, L.; Konotop, V. V.; Ye, F. Optical Soliton Formation Controlled by Angle Twisting in Photonic Moiré Lattices. Nat. Photonics 2020, 14 (11), 663–668.
- 28. Lyu, J.; Wen, Z.; Han, K.; Qi, X.; Gao, Y. Nonlinear Transmission and Pseudospin in Two-Dimensional Octagon and Dodecagon Photonic Lattices. Opt. Mater. Express 2018, 8 (9), 2713–2721.
- 29. Zeng, J.; Hu, Y.; Zhang, X.; Fu, S.; Yin, H.; Li, Z.; Chen, Z. Localization-to-Delocalization Transition of Light in Frequency-Tuned Photonic Moiré Lattices. Opt. Express 2021, 29 (16), 25388–25398.
- 30. Jin, W.; Song, M.; Xue, Y. L.; Gao, Y.; Zheng, L. Construction of Photorefractive Photonic Quasicrystal Microstructures by Twisted Square Lattices. Appl. Opt.2020, 59 (22), 6638–6641.
- 31. Sun, X.; Wu, F.; Wang, S.; Qi, Y.; and Zeng, Y. Design of Gradient Photonic Crystal Lens Array Using Two-Parameter Hexagonal Prism Interferometer, Acta Optica Sinica 2020, 40, 0222002.
- 32. Behera, S.; Joseph, J. Single-Step Optical Realization of Bio-Inspired Dual-Periodic Motheye and Gradient-Index-Array Photonic Structures. Opt. let. 2016, 41 (15), 3579–3582.
- 33. Ohlinger, K.; Lutkenhaus, J.; Arigong, B.; Zhang, H.; Lin, Y. Spatially Addressable Design of Gradient Index Structures through Spatial Light Modulator Based Holographic Lithography. J. Appl. Phys. 2013, 114 (21), 213102.
- 34. Lowell, D.; Lutkenhaus, J.; George, D.; Philipose, U.; Chen, B.; Lin, Y. Simultaneous Direct Holographic Fabrication of Photonic Cavity and Graded Photonic Lattice with Dual Periodicity, Dual Basis, and Dual Symmetry. Opt. Express 2017, 25 (13), 14444–14452.
- 35. Lowell, D.; Hassan, S.; Sale, O.; Adewole, M.; Hurley, N.; Philipose, U.; Chen, B.; Lin, Y. Holographic Fabrication of Graded Photonic Super-Quasi-Crystals with Multiple-Level Gradients. Appl. Opt. 2018, 57 (22), 6598–6604.
- 36. Alnasser, K.; Kamau, S.; Hurley, N.; Cui, J.; Lin, Y. Resonance Modes in Moiré Photonic Patterns for Twistoptics. OSA Continuum 2021, 4 (4), 1339–1347.
- 27. Lowell, D.; Hassan, S.; Adewole, M.; Philipose, U.; Chen, B.; Lin, Y. Holographic fabrication of graded photonic super-crystals using an integrated spatial light modulator and reflective optical element laser projection system. Appl. Opt. 2017, 56, 9888–9891.
- Hassan, S.; Sale, O.; Alnasser, K.; Hurley, N.; Zhang, H.; Philipose, U.; Lin, Y. Broadband Light-Matter Interaction Due to Resonance Cavities in Graded Photonic Super-Crystals. OSA Continuum 2019, 2 (11), 3272–3280.
- 39. Hassan, S.; Jiang, Y.; Alnasser, K.; Hurley, N.; Zhang, H.; Philipose, U.; Lin, Y. Generation of over 1000 Diffraction Spots from 2D Graded Photonic Super-Crystals. Photonics 2020, 7(2), 27.
- 40. Amidror, I. The Theory of the Moiré Phenomenon: Volume I: Periodic Layers, second edition (Springer 2009).

- 41. Johnson, S. G.; Joannopoulos, J. D. Block-Iterative Frequency-Domain Methods for Maxwell's Equations in a Planewave Basis. Opt. express 2001, 8 (3), 173–190.
- 42. Mandelshtam, V. A.; Taylor, H. S. Harmonic Inversion of Time Signals and Its Applications. J. Chem. Phys. 1997, 107, 6756–6769.
- 43. Oskooi, A. F.; Roundy, D.; Ibanescu, M.; Bermel, P.; Joannopoulos, J. D.; Johnson, S. G. MEEP: A Flexible Free-Software Package for Electromagnetic Simulations by the FDTD Method. Comput. Phys. Commun. 2010, 181 (3), 687–702.
- 44. Alnasser, K.; Hassan, S.; Kamau, S.; Zhang, H.; Lin, Y. Enhanced light extraction from organic light-emitting diodes by reducing plasmonic loss through graded photonic super-crystals. J. Opt. Soc. America B 2020, 37 (5), 1283-1289.
- 45. Barik, S.; Karasahin, A.; Flower, C.; Cai, T.; Miyake, H.; DeGottardi, W.; Hafezi, M.; and Waks, E. A topological quantum optics interface. Science 2018, 359, 666-668.
- 46. Shalaev, M.I.; Walasik, W.; Tsukernik, A.; Xu, Y.; and Litchinitse, N. M. Robust topologically protected transport in photonic crystals at telecommunication wavelengths. Nat. Nanotech. 2019, 14, 31–34.
- 47. Hassan, S.; Alnasser, K.; Lowell, D.; Lin, Y. Effects of Photonic Band Structure and Unit Super-Cell Size in Graded Photonic Super-Crystal on Broadband Light Absorption in Silicon. Photonics 2019, 6, 50. https://doi.org/10.3390/photonics6020050